

Contents lists available at ScienceDirect

Petroleum Science

journal homepage: www.keaipublishing.com/en/journals/petroleum-science



Original Paper

Quantitative evaluation of gas hydrate reservoir by AVO attributes analysis based on the Brekhovskikh equation



Yao Wang a, b, c, Yan-Fei Wang a, b, c, *

- ^a Key Laboratory of Petroleum Resources Research, Institute of Geology and Geophysics, Chinese Academy of Sciences, Beijing, 100029, China
- b University of Chinese Academy of Sciences, Beijing, 100049, China
- ^c Innovation Academy for Earth Science, Chinese Academy of Sciences, Beijing, 100029, China

ARTICLE INFO

Article history: Received 20 August 2021 Received in revised form 1 November 2022 Accepted 13 February 2023 Available online 22 February 2023

Edited by Jie Hao

Keywords:
Natural gas hydrate
Brekhovskikh equation
AVO attributes
Random forest

ABSTRACT

AVO (Amplitude variation with offset) technology is widely used in gas hydrate research. BSR (Bottom simulating reflector), caused by the huge difference in wave impedance between the hydrate reservoir and the underlying free gas reservoir, is the bottom boundary mark of the hydrate reservoir. Analyzing the AVO attributes of BSR can evaluate hydrate reservoirs. However, the Zoeppritz equation which is the theoretical basis of conventional AVO technology has inherent problems: the Zoeppritz equation does not consider the influence of thin layer thickness on reflection coefficients; the approximation of the Zoeppritz equation assumes that the difference of wave impedance between the two sides of the interface is small. These assumptions are not consistent with the occurrence characteristics of natural gas hydrate. The Brekhovskikh equation, which is more suitable for thin-layer reflection coefficient calculation, is used as the theoretical basis for AVO analysis. The reflection coefficients calculated by the Brekhovskikh equation are complex numbers with phase angles. Therefore, attributes of the reflection coefficient and its phase angle changing with offset are used to analyze the hydrate reservoir's porosity, saturation, and thickness. Finally, the random forest algorithm is used to predict the reservoir porosity, hydrate saturation, and thickness of the hydrate reservoir. In the synthetic data, the inversion results based on the four attributes of the Brekhovskikh equation are better than the conventional inversion results based on the two attributes of Zoeppritz, and the thickness can be accurately predicted. The proposed method also achieves good results in the application of Blake Ridge data. According to the method proposed in this paper, the hydrate reservoir in the area has a high porosity (more than 50%), and a medium saturation (between 10% and 20%). The thickness is mainly between 200m and 300m. It is consistent with the previous results obtained by velocity analysis.

© 2023 The Authors. Publishing services by Elsevier B.V. on behalf of KeAi Communications Co. Ltd. This is an open access article under the CC BY-NC-ND license (http://creativecommons.org/licenses/by-nc-nd/4.0/).

1. Introduction

At present, the exploration and identification of gas hydrate are mainly based on BSR identification, impedance inversion, velocity anomaly zone, and AVO analysis methods. Among them, AVO analysis has been widely used in the research of hydrate reservoir identification and internal structure analysis and has achieved good results. Ecker et al. (1998) predicted three variations on BSR by the

Zoeppritz equation based on the single-phase medium theory. Mallick et al. (2000) combined AVO analysis with mixed pre-stack and post-stack inversion to realize elastic impedance inversion of the hydrate reservoir. Andreassen et al. (1997) studied the BSR phenomenon at the bottom of the continental margin of the Beaufort Sea. Based on AVO analysis, Lu and Mcmechan (2004) used the sparse tip pulse-constrained inversion technique to invert seismic impedance and predict gas hydrate distribution in the Black Sea Platform. Yi and Lee (2011) used the conventional AVO analysis method to analyze BSR, and then qualitatively evaluate the concentration of NGH (Natural Gas Hydrate). With the application of AVO technology in hydrate reservoir identification, many scholars have motivated their research objectives from the qualitative identification of hydrates to quantitative analysis. Salehi et al.

^{*} Corresponding author. Key Laboratory of Petroleum Resources Research, Institute of Geology and Geophysics, Chinese Academy of Sciences, Beijing, 100029, China

 $[\]hbox{\it E-mail addresses: } wang_yao@mail.iggcas.ac.cn (Y. Wang), yfwang@mail.iggcas.ac.cn (Y.-F. Wang).$

(2013) used AVO technology to quantitatively analyze the hydrate saturation and free gas content of hydrate reservoirs near the BSR interface in offshore Iran. Yi et al. (2018) combined petrophysical modelling with pre-stack inversion to carry out a quantitative analysis of hydrate reservoirs in the waters of Japan. Arun et al. (2020) calculated hydrate saturation and free gas saturation in the Indian sea area through AVO inversion of 2D seismic records. The Zoeppritz equation and its approximation are the theoretical basis of the above-mentioned AVO research, and the assumptions applied in its theoretical analysis lead to the limitations of thinlayer studies. In this study, the Brekhovskikh equation, which is more suitable for calculating the reflection coefficient of thin layers, is used instead of the Zoeppritz equation to analyze various AVO attributes of BSR. The Brekhovskikh equation is proposed by the Soviet geophysicist Brekhovskikh (1987) which includes the correspondence of the interlayers' thicknesses to reflection coefficient

quantitatively analyze the thickness and microstructure of the hydrate reservoir.

2. Methodology

The method consists of AVO theory, extraction, analysis of AVO attributes (P1, G1, P2, G2), and prediction of porosity, saturation, and thickness by using the random forest algorithm.

2.1. AVO theory

The AVO analysis has been widely utilized as an effective reservoir characterization tool. The conventional AVO technology based on a single interface assumption can be completely described by the Zoeppritz equation (Zoeppritz, 1919)

$$\begin{bmatrix} \sin \theta_{1} \\ \cos \theta_{1} \\ \sin 2\theta_{1} \\ \cos 2\varphi_{1} \end{bmatrix} = \begin{bmatrix} -\sin \theta_{1} & -\cos \varphi_{1} & \sin \theta_{2} & \cos \varphi_{2} \\ \cos \theta_{1} & -\sin \varphi_{1} & \cos \theta_{2} & -\sin \varphi_{2} \\ \sin 2\theta_{1} & \frac{V_{P1}}{V_{S1}} \cos 2\varphi_{1} & \frac{\rho_{2}}{\rho_{1}} \frac{V_{P1}}{V_{P2}} \frac{V_{S2}^{2}}{V_{S1}^{2}} \sin 2\theta_{2} & \frac{\rho_{1}}{\rho_{2}} \frac{V_{P1}}{V_{S1}} \frac{V_{S2}}{V_{S1}} \cos 2\varphi_{2} \\ -\cos 2\varphi_{1} & \frac{V_{S1}}{V_{P1}} \sin 2\varphi_{1} & \frac{\rho_{2}}{\rho_{1}} \frac{V_{P2}}{V_{S1}} \cos 2\varphi_{2} & -\frac{\rho_{2}}{\rho_{1}} \frac{V_{S2}}{V_{P1}} \sin 2\varphi_{2} \end{bmatrix} \begin{bmatrix} R_{PP} \\ R_{PS} \\ T_{PP} \\ T_{PS} \end{bmatrix}$$

$$(1)$$

and AVO attributes. Hence, the Brekhovskikh equation is more suitable for thin-layer AVO research and should be used instead of the Zoeppritz equation, to solve the problems existing in the thinlayer AVO technology on a theoretical basis. Wang (2006) compared the results of the Brekhovskikh equation and the Zoeppritz equation within thin-layer media and concluded that the former is more suitable for AVO inversion in thin-layer media. Lu (2013) employed the forward modelling data with this equation as the theoretical guidance of AVO research, and the results showed that the forward modelling data of this equation was closer to the actual situation. Chen et al. (2020) used the Brekhovskikh equation to analyze the influence of seismic wave interference in thin interbedding on AVO attributes, the phase angle of the reflection coefficients is not involved in their study, and the purpose is different from this paper. The reflection coefficient calculated by the Brekhovskikh equation is complex, so there is a phase angle in the reflection coefficient. At present, there are few studies on the change of reflection coefficient phase angle with offset, so it is very necessary to calculate the reflection coefficient phase angle for studying thin reservoir or wide-angle seismic reflection (Meng et al., 2010).

BSR can mark the bottom interface of the hydrate reservoir due to the huge difference in wave impedance between the hydrate reservoir and the underlying free gas reservoir. It is usually difficult to determine the interface of the hydrate top. The thickness of the hydrate reservoir can be estimated by taking the Brekhovskikh equation with considering the thickness factor as the theoretical basis for the AVO attributes analysis of the hydrate reservoir. In this paper, the conventional AVO analysis method considering only the reflection coefficient intercept and gradient attributes is developed into a new AVO attributes analysis method considering both the reflection coefficient intercept-gradient attributes (P1-G1) and the reflection coefficient phase angle intercept-gradient attributes (P2-G2). Finally, AVO attributes analysis based on the Brekhovskikh equation is combined with the random forest algorithm to

where V_{P1} and V_{P2} are the P-wave velocities of two layers, respectively; V_{S1} and V_{S2} are the S-wave velocities of two layers; ρ_1 and ρ_2 are the density of two layers; θ_1 and θ_2 are the reflection angle and transmission angle of the P-wave respectively. φ_1 and φ_2 are reflection angle and transmission angle of the S-wave respectively. Before the development of computing power, the Zoeppritz equation was complex, so many linear approximate equations were developed. Among these approximate equations, the Shuey equation (Shuey, 1985) is the representative of AVO attributes analysis

$$R(\theta) = R_0 + \left[A_0 R_0 + \frac{\Delta \sigma}{(1 - \sigma)^2} \right] \sin^2 \theta + \frac{1}{2} \frac{\Delta V_P}{V_P} \left(\tan^2 \theta - \sin^2 \theta \right)$$
 (2)

where, $R_0 = \frac{1}{2} \left(\frac{\Delta V_P}{V_P} + \frac{\Delta \rho}{\rho} \right)$, $A_0 = B_0 - 2(1 + B_0) \left(\frac{1-2\sigma}{1-\sigma} \right)$, $B_0 = \frac{\Delta V_P}{V_P} / \left(\frac{\Delta V_P}{V_P} + \frac{\Delta \rho}{\rho} \right)$; θ is the angle of incidence; R_0 is the reflection coefficient at zero degree incidence; V_P is the P-wave velocity of the medium below the interface; ΔV_P is the velocity difference between two layers of media; σ is the Poisson ratio of the medium below the interface; $\Delta \sigma$ is the Poisson ratio difference of two-layer medium; ρ is the density of the medium below the interface; $\Delta \rho$ is the density difference between the two layers of media.

The above two equations are based on the single interface assumption, ignoring the influence of stratum thickness on reflection coefficients. Shuey's equation requires that the wave impedance difference between the two layers is small in the calculation process, which does not accord with the reality that BSR is a strong impedance reflection interface. Therefore, in this paper, the Brekhovskikh equation considering physical parameters and thickness is used to analyze AVO attributes. The formula for calculating P-wave reflection coefficients based on the Brekhovskikh equation is:

(3)

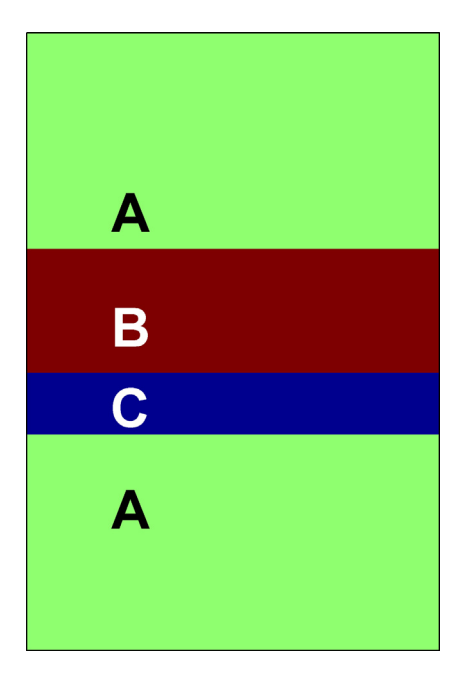


Fig. 1. Natural gas hydrate model.

2.2. Extraction and analysis of AVO attributes

In the conventional AVO attribute analysis methods, interceptgradient attributes are often regarded as important attributes of reservoir analysis. In the calculation of reflection coefficients, the Brekhovskikh equation can obtain the variation regulation of the reflection coefficient phase angle with offset. Therefore, this paper develops an AVO attributes analysis method that comprehensively considers the intercept-gradient attributes of reflection coefficients (P1-G1) and the intercept-gradient attributes of the reflection coefficient phase angles (P2-G2).

Robinson (1967) proposed a classical convolution model, which uses a seismic wavelet and reflection coefficients convolution to obtain seismic records:

$$S(t) = w(t) * r(t) \tag{4}$$

In equation (4), s(t) is the seismic data, w(t) is the seismic wavelet, r(t) is the seismic reflectivity, * represents the convolution operation. Performing Hilbert transforms to both sides of Eq. (4) yields:

$$\widetilde{s}(t) = \frac{1}{\pi} \int_{-\infty}^{\infty} \frac{s(\tau)}{t - \tau} d\tau = \frac{1}{\pi} \int_{-\infty}^{\infty} \int_{-\infty}^{\infty} \frac{w(\eta)r(\tau - \eta)}{t - \tau} d\eta d\tau$$

$$= \int_{-\infty}^{\infty} w(\eta) \frac{1}{\pi} \int_{-\infty}^{\infty} \frac{r(\tau - \eta)}{t - \tau} d\tau d\eta$$
(5)

In which, $\tilde{s}(t)$ is the Hilbert transform of s(t). Assuming $\xi = \tau - \eta$:

$$\widetilde{s}(t) = \int_{-\infty}^{\infty} w(\eta) \frac{1}{\pi} \int_{-\infty}^{\infty} \frac{r(\xi)}{(t-\eta) - \xi} d\xi d\eta = \int_{-\infty}^{\infty} w(\eta) \widetilde{r}(t-\eta) d\eta$$

$$= w(t) *\widetilde{r}(t)$$
(6)

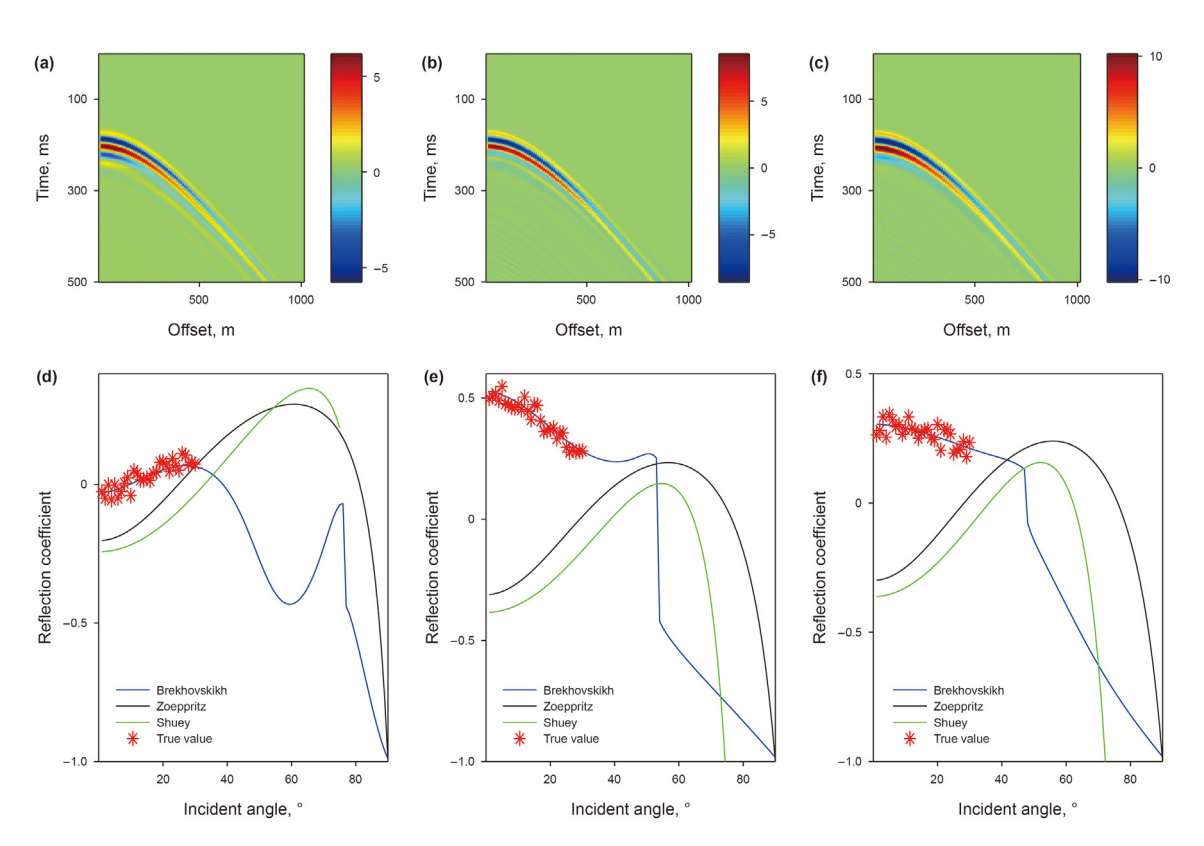


Fig. 2. (a) The synthetic data based on model 1. (b) The synthetic data based on model 2. (c) The synthetic data based on model 3. (d) Comparison of true reflection coefficients of model 1 with theoretical solutions of three equations. (e) Comparison of true reflection coefficients of model 2 with theoretical solutions of three equations. (f) Comparison of true reflection coefficients of model 3 with theoretical solutions of three equations.



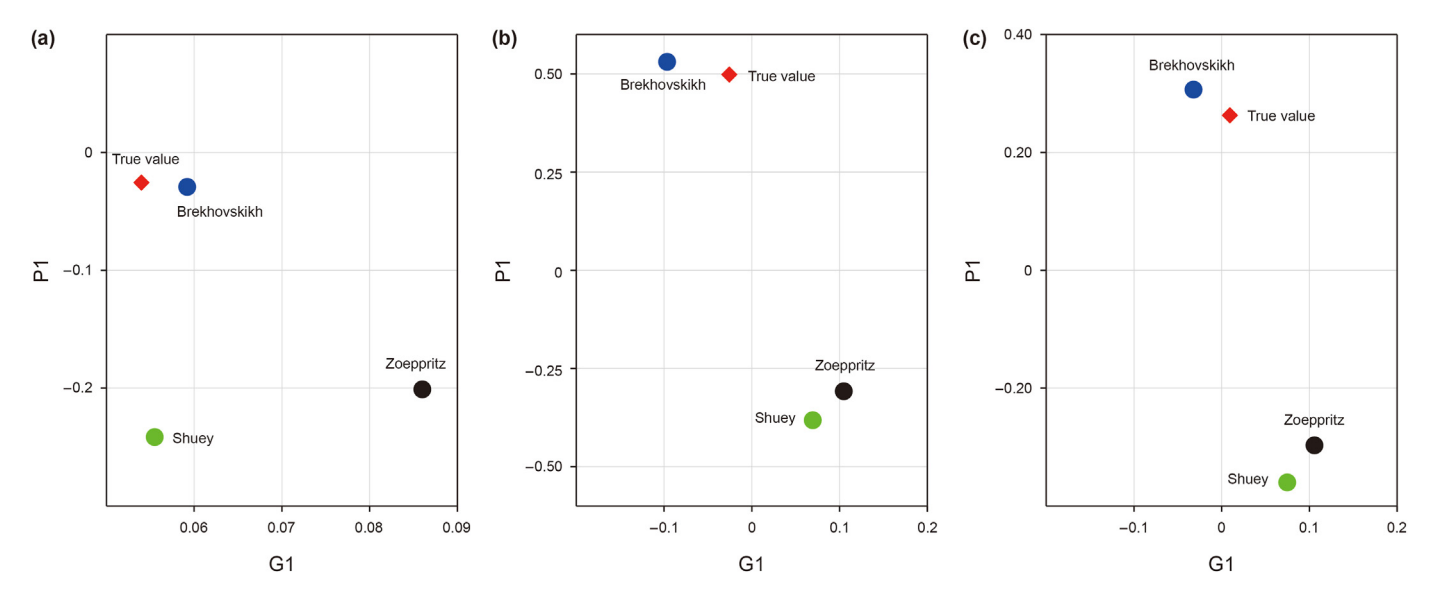


Fig. 3. Comparison of intercept-gradient attributes of reflection coefficients obtained from seismic records with theoretical solutions calculated by three equations (a) model 1, (b) model 2, and (c) model 3.

As the convolution operation satisfies commutative and associative laws we have

$$\widetilde{s}(t) = w(t) * \widetilde{r}(t) = w(t) * r(t) * \frac{1}{\pi t} = w(t) * \frac{1}{\pi t} * r(t) = \widetilde{w}(t) * r(t)$$
(7)

In which, $\tilde{w}(t)$ and $\tilde{r}(t)$ are Hilbert transforms of w(t) and r(t), respectively. Using the sparse regularization technique (Wang et al., 2011) to deconvolute complex seismic records with L1 norm constraints, the reflection coefficients in the complex form can be obtained, and the intercept-gradient attributes of reflection coefficients (P1-G1) and the intercept-gradient attributes of reflection coefficient phase angle (P2-G2) can be obtained.

Three hydrate reservoirs with different thicknesses, porosity, and saturation are established through hydrate petrophysical theory (Appendix A). The structure of the three models is similar and is shown in Fig. 1.

Stratum A is an ordinary submarine sediment layer, the P-wave velocity is 1717 m/s, the S-wave velocity is 600 m/s, and the density is 1.59 g/cm³. Stratum B is a natural gas hydrate reservoir. Stratum C is rich in free gas, the P-wave velocity is 1681.60 m/s, the S-wave velocity is 592.71 m/s, and the density is 1.52 g/cm³. In model 1, the thickness of stratum B is 30 m, the P-wave velocity is 1768 m/s, the S-wave velocity is 1005 m/s, and the density is 2.18 g/cm³. In model 2, the thickness of stratum B is 20 m, the P-wave velocity is 2136 m/s, the S-wave velocity is 1220 m/s, and the density is 2.28 g/cm³. In model 3, the thickness of stratum B is 10 m, the P-wave velocity is 2325 m/s, the S-wave velocity is 1361 m/s, and the density is 2.04 g/cm³.

The elastic wave forward modelling is carried out for the above three models. The forward equation of elastic wave (Tessmer et al., 1992) is:

$$\nabla^2 f - \frac{1}{C^2} \frac{\partial^2 f}{\partial t^2} = -\frac{1}{C^2} F \tag{8}$$

In which, f is the displacement position, C is the P-wave velocity or S-wave velocity, t is the time, and F is the source function. The forward modelling steps are realized following the procedure of Tesseral software: the zero-phase wavelet with the dominant frequency of 30 Hz is used as the source pulse, the time sampling

interval is 2 ms, the channel interval is 10 m, and the total number of channels is 100. Seismic data are obtained by elastic wave forward modelling. BSR reflection interfaces are extracted from seismic data, as shown in Fig. 2 (a), (b), and (c). Extracting the BSR reflection coefficients and comparing them with the theoretical results calculated by the Brekhovskikh equation, Zoeppritz equation, and Shuey equation, are shown in Fig. 2 (d), (e), and (f).

By comparing the reflection coefficients extracted by the above three models in seismic data with the theoretical results calculated by the three equations, the Brekhovskikh equation has higher accuracy for thin layers. When the incident angle is too large, the Shuey equation cannot calculate the reasonable reflection coefficients, so it is not drawn completely.

The reflection coefficients intercept-gradient attributes (P1-G1) are extracted from the above three models and compared with the theoretical values calculated by the three equations. P1 is the reflection coefficient when the incident angle is 0°. G1 is the slope of the reflection coefficients curve from 0 to 15°. The Brekhovskikh equation shows better consistency for P1-G1 attributes, as is shown in Fig. 3.

The variation of the reflection coefficients phase angle with offset is closely related to the thin layer thickness. Based on the Hilbert transform and the sparse regularization technique, the intercept-gradient attributes of BSR's reflection coefficients phase angle in the above three seismic records are extracted and compared with the theoretical results of different thicknesses calculated by the Brekhovskikh equation, as is shown in Fig. 4.

As shown in Fig. 5, P2 is the reflection coefficient phase angle when the incident angle is 0°. G2 is the slope of the reflection coefficients phase angle curve from 0 to 15°. P2-G2 can describe the thickness well, so the intercept-gradient attributes of reflection coefficients phase angle (P2-G2) can be used as an important indicator of thin layer thickness.

The above four AVO attributes (P1-G1 and P2-G2) are used to identify the porosity, saturation, and thickness of hydrate reservoirs.

2.3. Prediction of reservoir parameters: random forest algorithm

The random forest method is a typical representative of the boosting method (Breiman, 2001), which is an ensemble learning

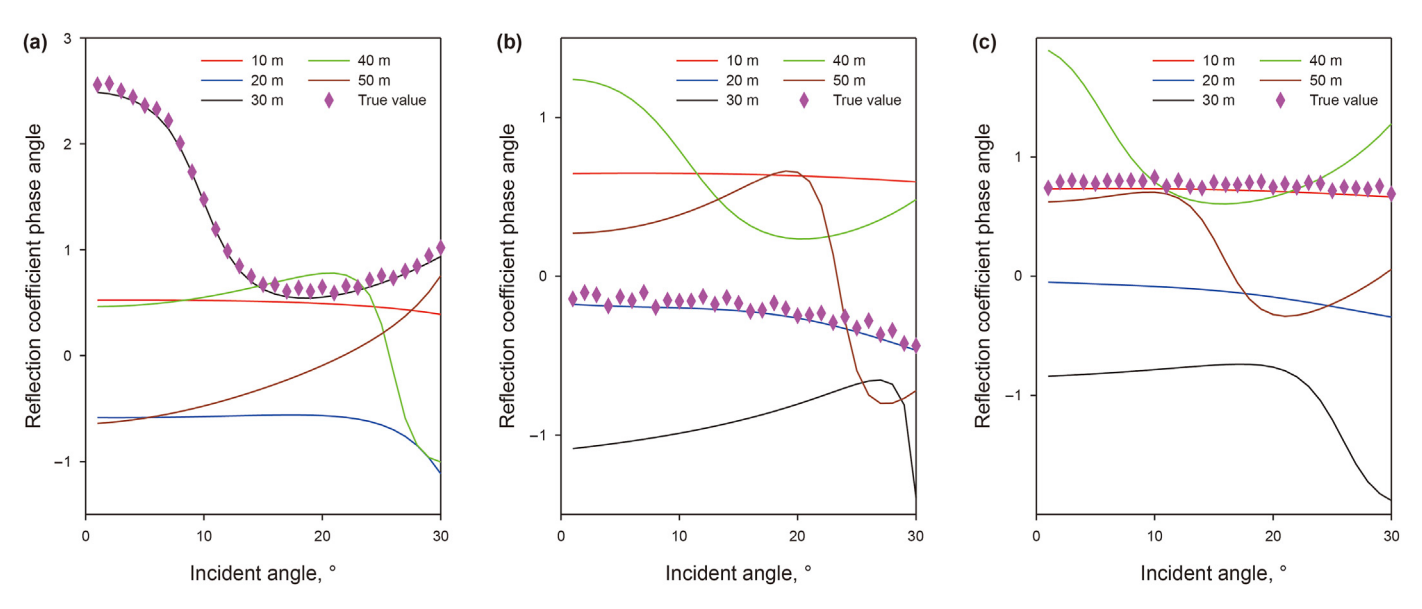


Fig. 4. Comparison of reflection coefficients phase angle obtained from seismic data with theoretical solutions calculated by the Brekhovskikh equation: (a) model 1, (b) model 2, (c) model 3.

method using decision trees as the base model. Fig. 6 is an illustration of the random forest method.

Random forest algorithm is developed based on decision tree theory and can be regarded as the combination of multiple decision trees. In a random forest, each decision tree is randomly generated and independent of the others. Multiple random trees in the forest vote together to determine the classification results of input samples. The decision tree of the random forest algorithm is defined as:

$$\{f(X_k, \delta_k), k = 1, 2, \dots, n\}$$
 (9)

In which, the variable k is the number of samples after resampling; X_k is a collection of input vectors, with each vector containing four AVO attributes extracted based on Brekhovskikh equation, P1, P2, G1 and G2; $f(X_k, \delta_k)$ is the basic classifier of the sub-decision tree; δ_k is a collection of labelled values corresponding to X_k , with each labelled value representing a variation of porosity, hydrate

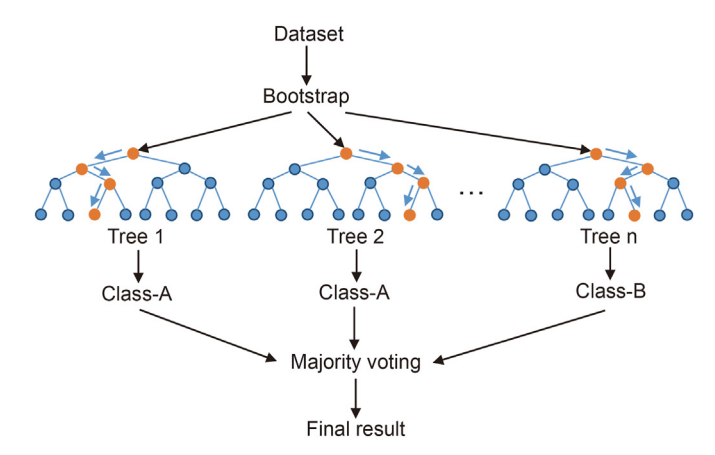


Fig. 6. Simplification of random forest.

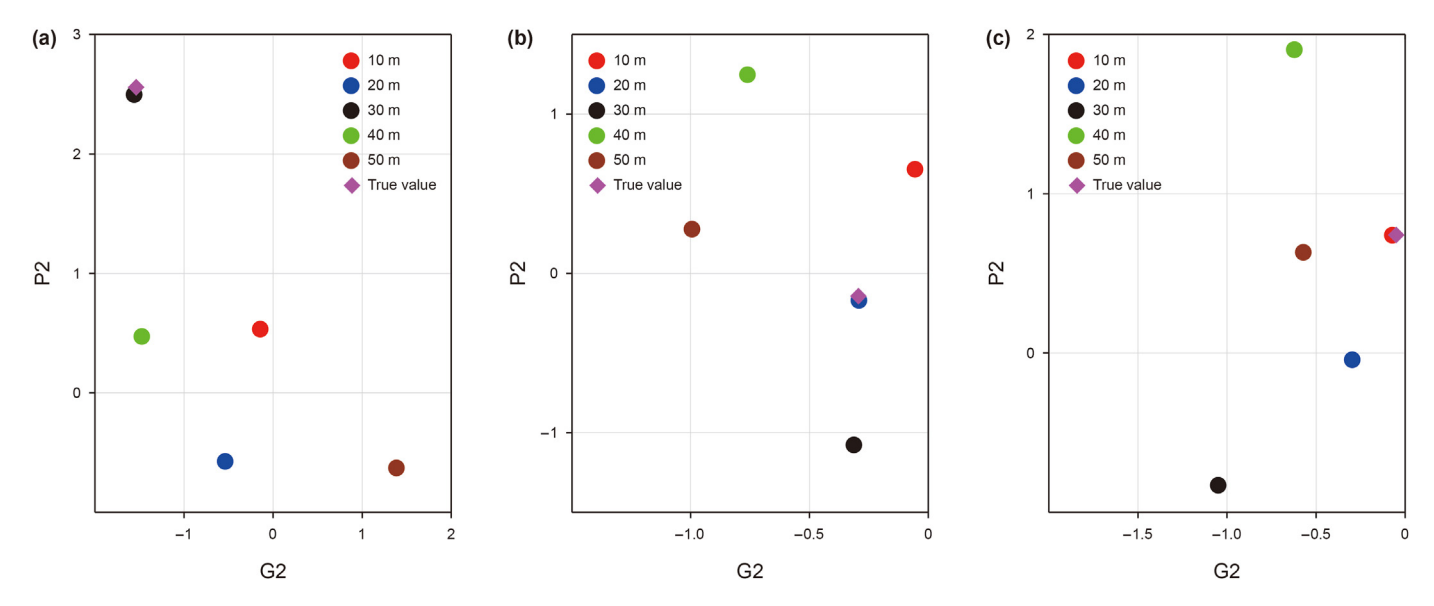


Fig. 5. Comparison of P2-G2 obtained from seismic data with theoretical solutions calculated by the Brekhovskikh equation: (a) model 1, (b) model 2, (c) model 3.

saturation or thickness.

To obtain a comprehensive training set, a series of gas hydrate reservoir models are established considering the porosity, saturation, and thickness of the gas hydrate reservoir. The variation range of reservoir porosity is between 5% and 70%, and the change step size is 1%. The hydrate saturation varies from 0 to 30% with a step size of 1%, and the thickness varies from 5 m to 550 m. Based on the petrophysical theory of natural gas hydrate, the P-wave velocity, S-wave velocity, and density of the hydrate reservoir can be obtained. The parameters of the overlying seafloor sedimentary layer and the underlying free gas layer are the same as stratum A and stratum C. Brekhovskikh equation is used to carry out BSR's AVO forward modelling on the above 39000 sets of data, and four AVO attributes

P1, G1, P2, and G2 defined as above are extracted. The variation tendency of the four AVO attributes with porosity, hydrate saturation, and reservoir thickness is shown in Fig. 7.

Referring to the classical machine learning experiment of IRIS recognition, porosity, saturation, and thickness are classified and labelled according to different intervals. Label values of the output parameters of our experiment are shown in Table 1. Porosity is divided into three intervals: low porosity (5%–25%) labelled 0; medium porosity (25%–50%) labelled 1; high porosity (50%–70%) labelled 2. Saturation is also divided into three intervals: low saturation (0%–10%) labelled 0; medium saturation (10%–20%) labelled 1; high saturation (20%–30%) labelled 2.

Two groups of attributes and corresponding labels are shown in

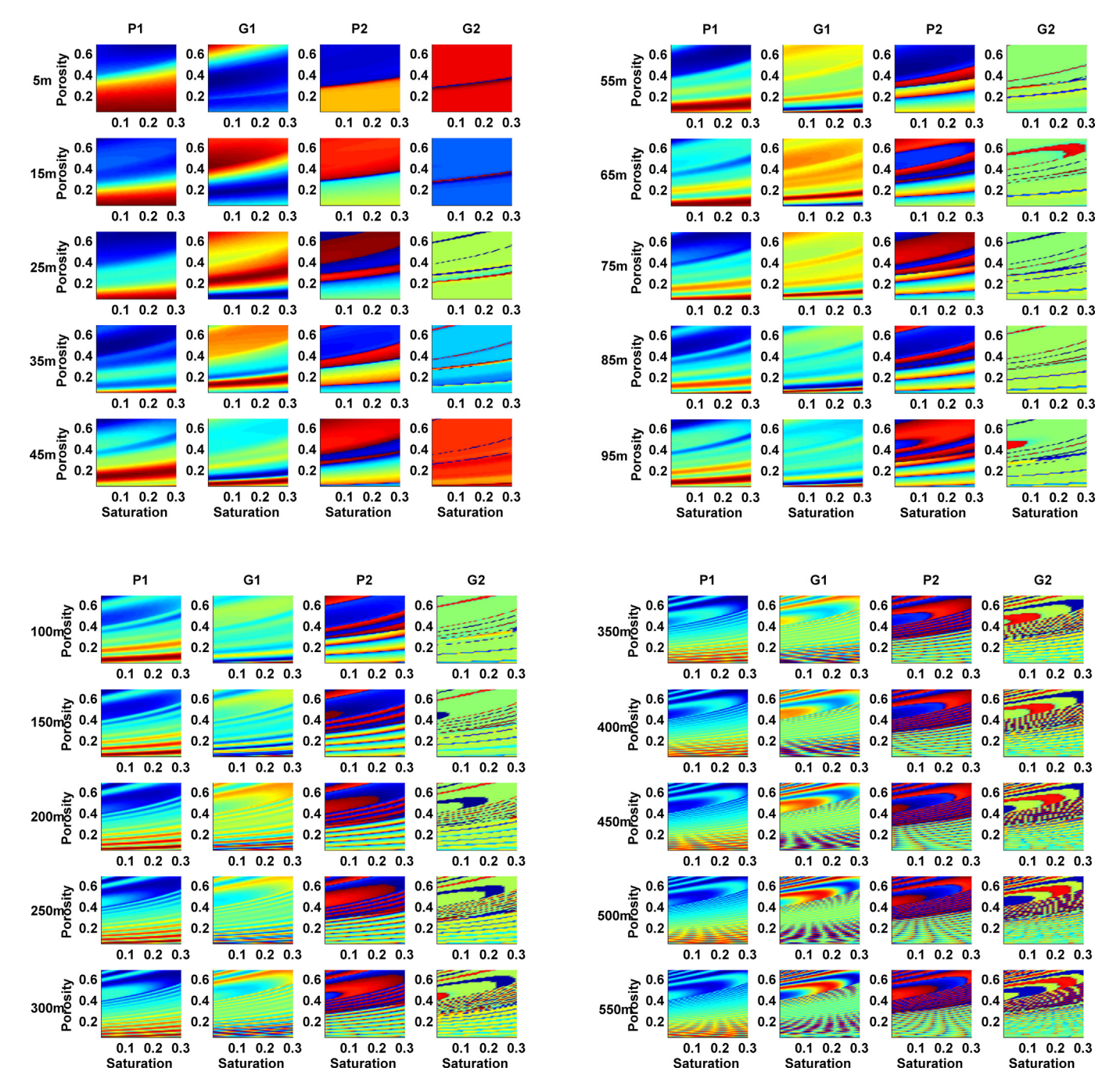


Fig. 7. The variation tendency of P1, G1, P2, and G2 with hydrate reservoir thickness, porosity, and hydrate saturation.

Table 1Output label values for reservoir porosity, hydrate saturation, and thickness.

Reservoir parameters	Range of parameters	Label value
Reservoir porosity	5%-25%	0
	25%-50%	1
	50%-75%	2
Hydrate saturation	0-10%	0
	10%-20%	1
	20%-30%	2
Reservoir thickness	5 m	0
	15 m	1
	25 m	2
	35 m	3
	45 m	4
	55 m	5
	65 m	6
	75 m	7
	85 m	8
	95 m	9
	100 m	10
	150 m	11
	200 m	12
	250 m	13
	300 m	14
	350 m	15
	400 m	16
	450 m	17
	500 m	18
	550 m	19

Fig. 8. The label values [1,1,0] represent a thin hydrate reservoir with medium porosity, medium saturation, and thickness of nearly 5 m. Label values [2,1,3] represent a hydrate reservoir with high porosity, medium saturation, and thickness of nearly 35 m.

To compare the predictions of the Brekhovskikh equation and the Zoeppritz equation, the training data set based on the Zoeppritz equation is also prepared. AVO forward modelling based on the Zoeppritz equation is carried out for the above series of models, and the reflection coefficients intercept-gradient attributes are extracted, as shown in Fig. 9. Reflection coefficients calculated based on the Zoeppritz equation do not change with the thickness, and the phase angle information of the reflection coefficients cannot be

obtained. Therefore, only two attributes can be used to estimate hydrate reservoir parameters.

3. Synthetic example

When predicting hydrate reservoir parameters, firstly, the BSR response is extracted from seismic data. Then, the complex reflection coefficients and attributes P1, G1, P2, and G2 are obtained through Hilbert transformation and sparse deconvolution. Finally, reservoir parameters are predicted based on the trained random forest model. Fig. 10 illustrates the flow chart of the proposed method.

In the process of synthetic example, three natural gas hydrate reservoirs as shown in Table 2 are established. When designing the thickness of the model, we take the label value of the nearest thickness as the model thickness label. To verify the anti-noise performance of the proposed method, seismic data with different signal-to-noise ratios (S/N = 100, S/N = 10, and S/N = 5) are obtained by forwarding modelling shown in Fig. 11.

For BSR with S/N=5, the method of adjacent channels stacking is used to suppress random noise. The P1-G1 and P2-G2 attributes of BSR are extracted and shown in Fig. 12. The four attributes extracted from seismic data with different S/N can match the theoretical values calculated by the Brekhovkikh equation well, which provides a good data basis for estimating reservoir porosity, saturation, and thickness. The P2-G2 attribute possesses better noise resistance. The P1-G1 attributes of seismic records with S/N=100 are used as inputs to predict porosity and saturation based on the Zoeppritz equation. Estimate reservoir parameters using the above attributes and compare the predicted results of the two mentioned equations. The predictions are shown in Table 3, Table 4, and Table 5.

The category prediction results of porosity are shown in Table 3. For different S/N, the predictions of porosity category based on the Brekhovskikh equation have an excellent effect. Among the results based on the Zoeppritz equation, only one is accurate. The category predictions of saturation are shown in Table 4. When S/N = 100 and 10, the predictions of saturation category based on the Brekhovskikh equation are accurate. When S/N = 5, two predictions of

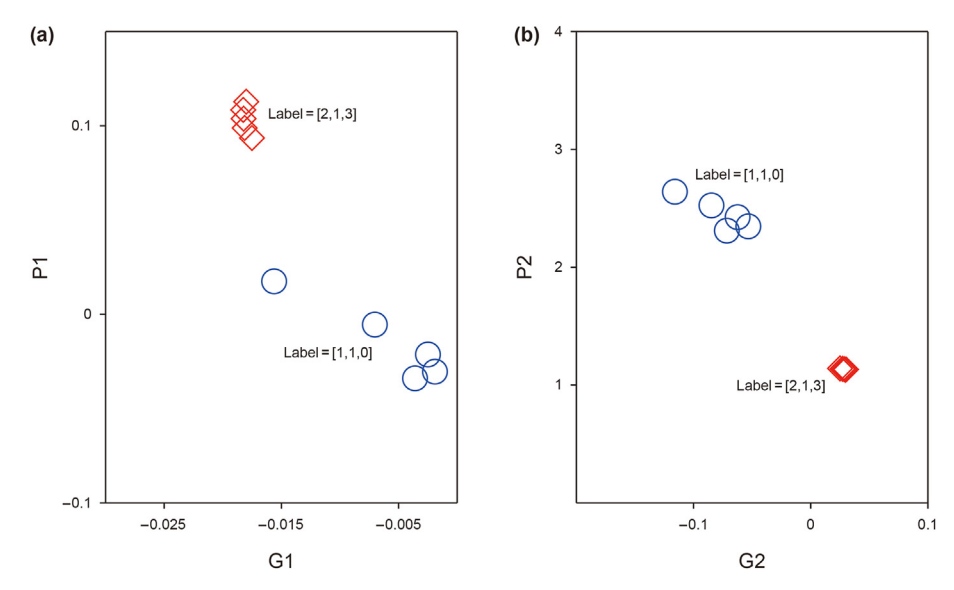


Fig. 8. Attributes and corresponding labels of P1-G1 and P2-G2.

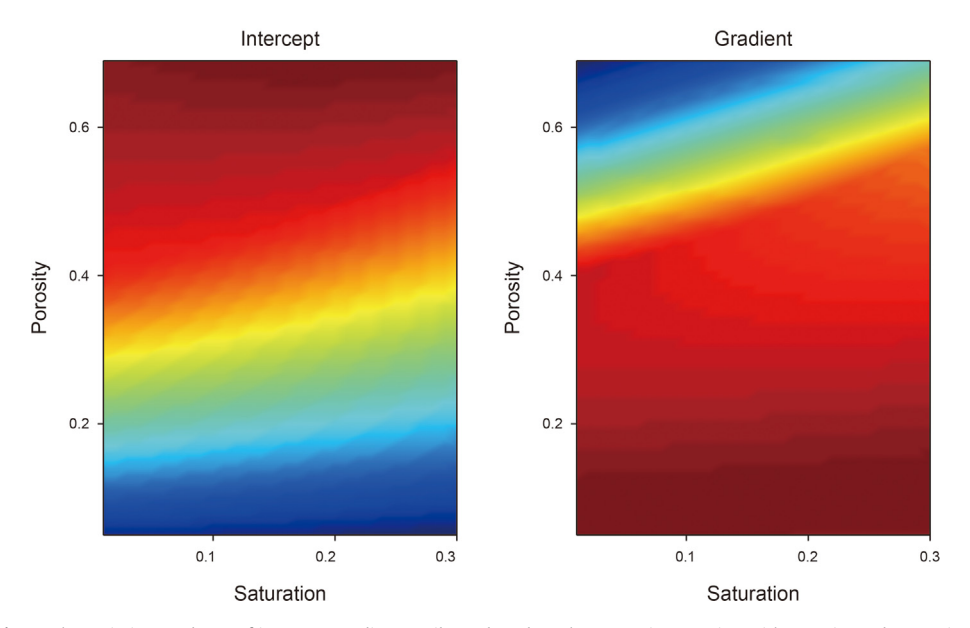


Fig. 9. The variation tendency of intercept-gradient attributes based on the Zoeppritz equation with porosity and saturation.

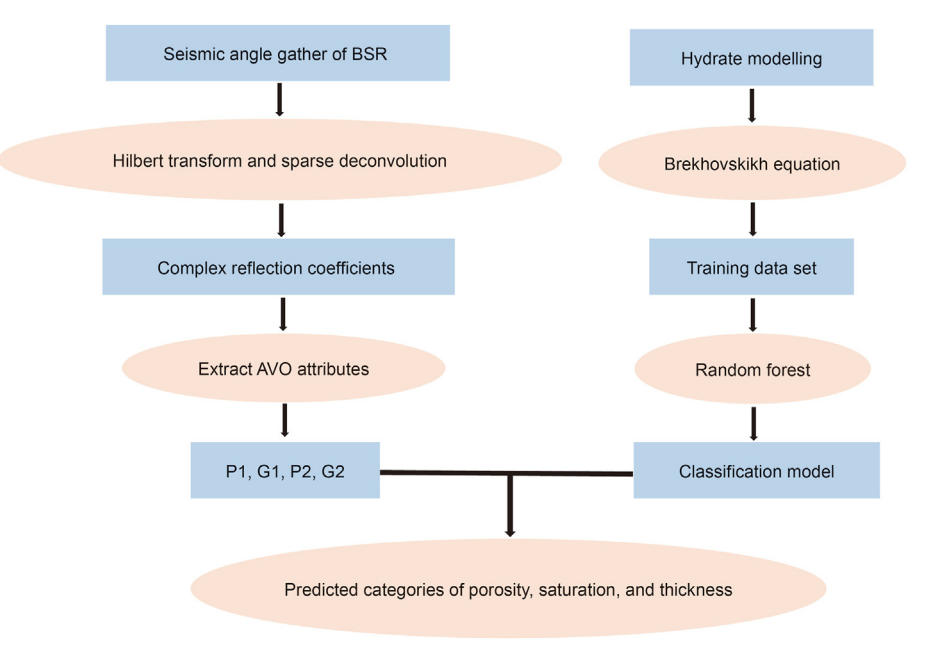
them are biased which indicates that saturation is sensitive to noise. The classification prediction results of thickness are shown in Table 5. When S/N=100 and 10, the predictions of thickness category based on the Brekhovskikh equation are accurate. When S/N=5, one of the predictions are biased, and the deviation is 1. This inidcates the feasibility and effectiveness of the proposed method.

4. Field data

The Blake Ridge area of the United States is one of the earliest areas to detect hydrate. After preprocessing the seismic records in this area, the common angle gathers shown in Fig. 13 are obtained. The 200th to 249th channels with obvious BSR response are

extracted, and the above four attributes P1-G1 and P2-G2 are extracted shown in Fig. 14. We compare the results based on the above two mentioned equations in Fig. 15.

The prediction results are the categories of the three parameters, and the approximate estimates of the three parameters can be obtained by referring to Table 1. Based on the Brekhovskikh equation, the following results are obtained: the hydrate reservoir in the area has a high porosity (more than 50%), and a medium saturation (between 10% and 20%). The thickness is mainly between 200 m and 300 m. This is basically in line with the conclusion drawn by Ecker (Ecker et al., 2000) with velocity analysis in this area. Hence this method based on the Brekhovskikh equation can be used for quantitative estimation of hydrate reservoirs.



 $\textbf{Fig. 10.} \ \ \textbf{Flow chart of quantitatively evaluate hydrate reservoir.}$

Table 2Model parameters and label values used to detect the accuracy of new methods.

Serial number	Porosity	Saturation	Thickness	Label value
A	12%	18%	12 m	[0,1,1]
В	30%	8%	7 m	[1,0,0]
C	60%	25%	23 m	[2,2,2]

5. Conclusion

In applying the Brekhovskikh equation to AVO forward modelling, the reservoir thickness is an essential factor affecting the AVO

attributes of BSR. Therefore, it is a tendency toward reservoir quantitative analysis to use the Brekhovskikh equation as the theoretical basis for AVO analysis of unconventional thin oil reservoirs like gas hydrate. The AVO intercept-gradient (P-G) method in conventional AVO attributes analysis is extended to the new AVO intercept-gradient (P1-G1 and P2-G2) approach, which considers the reflection coefficients and the reflection coefficients phase angle. The AVO attributes information on BSR is widely accepted, and the influence of reservoir thickness is reflected in AVO attributes. Referring to the classical machine learning experiment of IRIS recognition, the random forest algorithm is used to predict the thickness, porosity, and hydrate saturation. The data experiment achieves a good prediction effect and provides a new idea for quantitative analysis of unconventional thin oil or gas reservoirs.

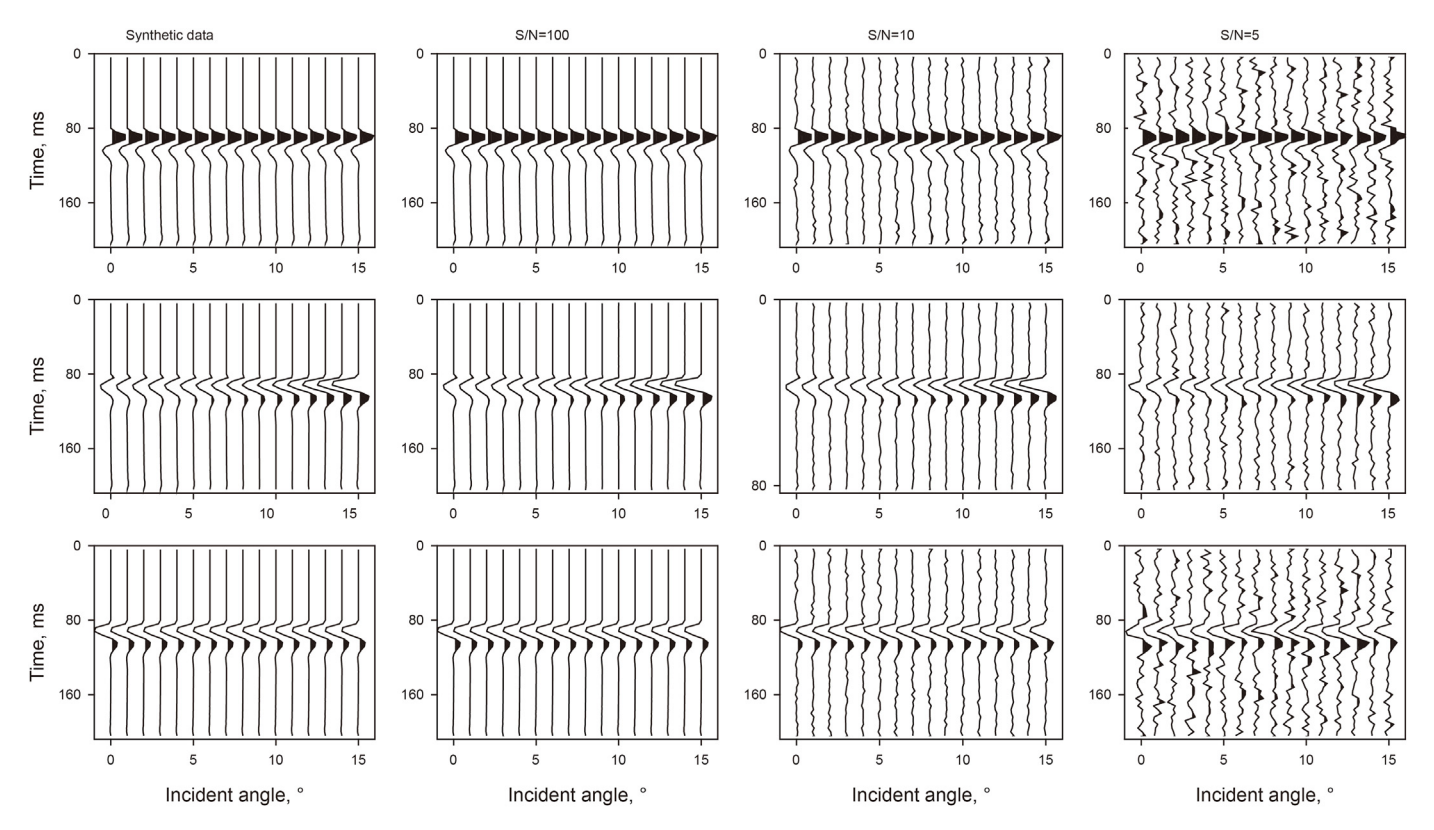


Fig. 11. Synthetic seismic data with different signal-to-noise ratios.

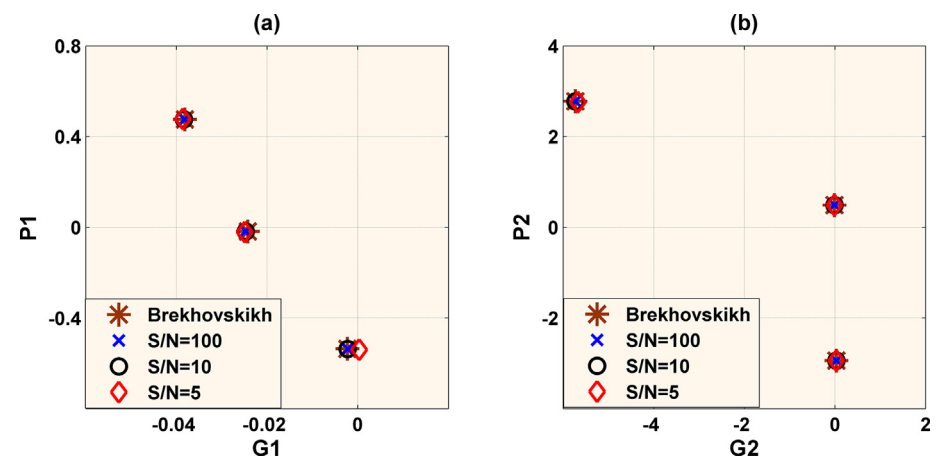


Fig. 12. Four attributes extracted from seismic data with different S/N are compared with the calculated values of the Brekhovskikh equation.

Table 3 Prediction results of porosity category.

Serial number	Porosity	Label value	S/N = 100	S/N = 10	S/N = 5	Zoeppritz
A	12%	0	0	0	0	2
В	30%	1	1	1	1	1
C	60%	2	2	2	2	1

Table 4 Prediction results of saturation category.

Serial number	Saturation	Label value	S/N = 100	S/N = 10	S/N = 5	Zoeppritz
A	18%	1	1	1	2	2
В	8%	0	0	0	1	1
C	25%	2	2	2	2	2

Table 5 Prediction results of thickness category.

Serial number	Thickness	Label value	S/N = 100	S/N = 10	S/N = 5
A	12m	1	1	1	1
В	7m	0	0	0	0
С	23m	2	2	2	1

Declaration of competing interest

The authors declare that they have no known competing financial interests or personal relationships that could have appeared to influence the work reported in this paper.

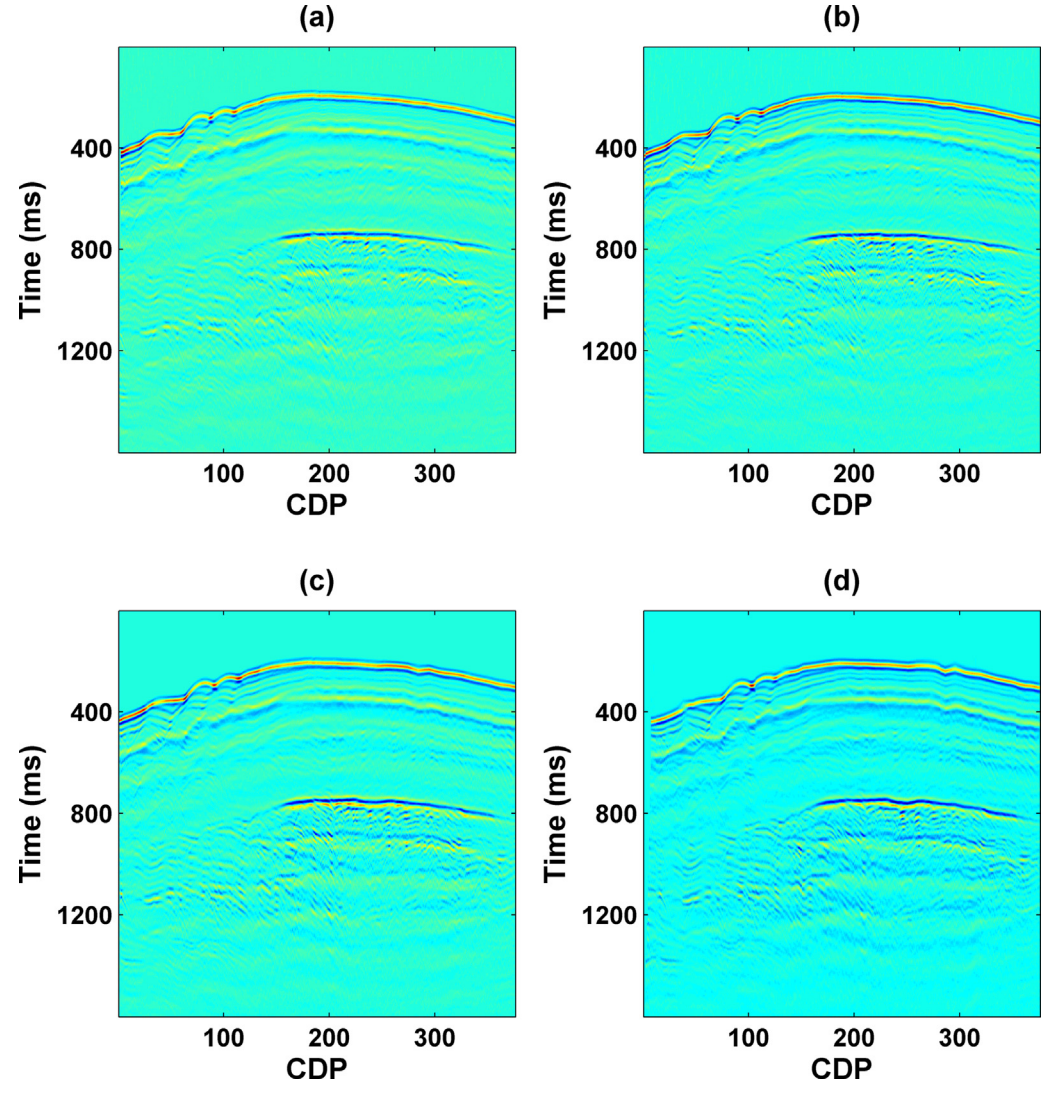


Fig. 13. (a) 0-degree angle gathers; (b) 5-degree angle gathers; (c) 10-degree angle gathers; (d) 15-degree angle gathers.

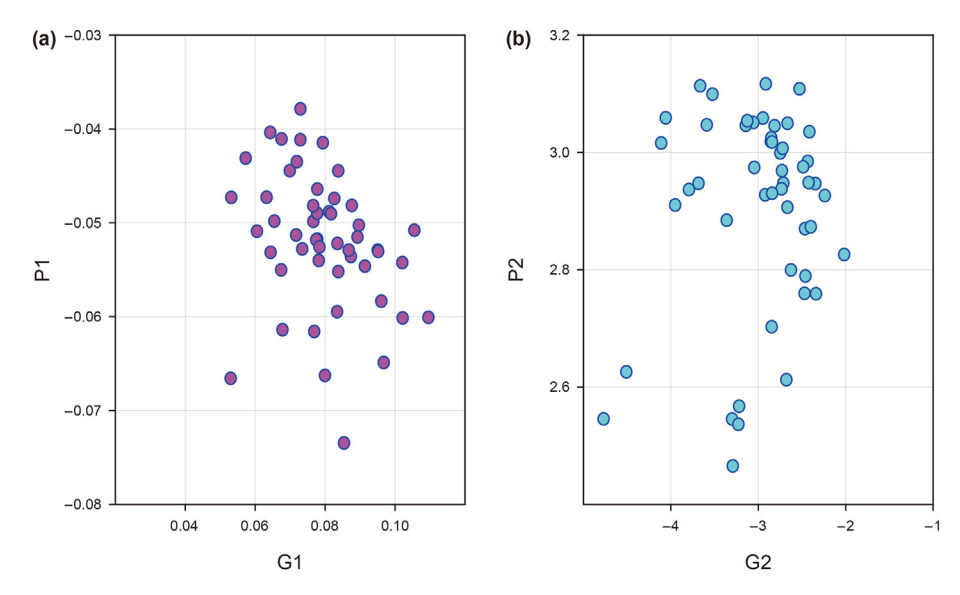


Fig. 14. Four attributes extracted from seismic data of the Blake Ridge area.

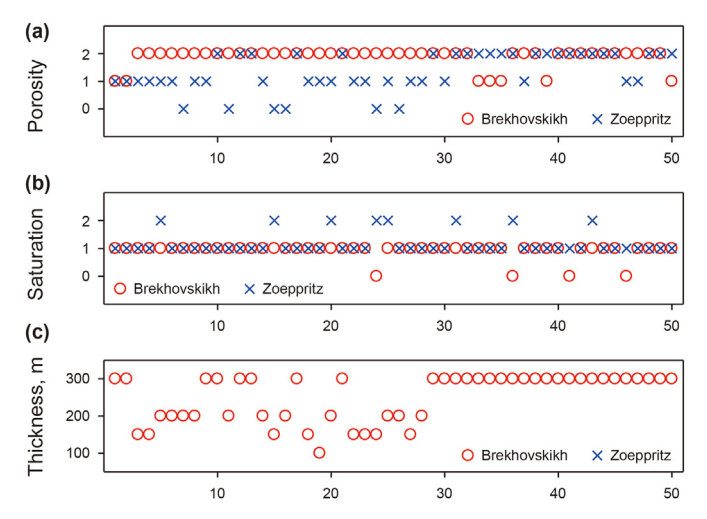


Fig. 15. Prediction of porosity, saturation, and thickness of Blake Ridge: (a) Porosity, (b) Saturation, and (c) Thickness.

Acknowledgements

We are grateful for constructive comments from reviewers, which improve the quality of the paper. The research is funded by the National Natural Science Foundation of China (No. 12171455), the Original Innovation Research Program of the Chinese Academy of Sciences (CAS) under grant number ZDBS-LY-DQC003, and the Key Research Programs IGGCAS-2019031.

Appendix A. Petrophysical theory of natural gas hydrate

In modelling the natural gas hydrate, the hydrate reservoir consists of solid, liquid, and gas phases. The solid rock skeleton contains a variety of mineral components. The petrophysical parameters and percentage content of various minerals are shown in Table A-1. There are N kinds of minerals that make up rocks. The proportion of each mineral is f_i (i=1, 2, ..., N). If the elastic modulus of each mineral M_i (M representing the bulk modulus K or the shear modulus G) is known, then the elastic modulus of the rock can be estimated according to the following two formulae:

Reuss formula (Reuss, 2006):

Table A-1
Petrophysical parameters of each component in model construction

Ingredient	Bulk modulus	Shear modulus	Density	Content
	K, Gpa	μ, Gpa	ρ , g/cm ³	
Calcite	76.8	32	2.71	35%
Clay	20.9	6.85	2.58	60%
Quartz	36	45	2.65	5%
Seawater	2.5	0	1.032	S_{w}
Natural gas hydrate	5.6	2.4	0.9	S_{h}

$$\frac{1}{M_R} = \sum_{i=1}^N \frac{f_i}{M_i} \tag{A-1}$$

Voigt formula (Voigt, 1889):

$$M_V = \sum_{i=1}^N f_i M_i \tag{A-2}$$

The modulus obtained by Voigt is the upper limit of the actual value, and the modulus obtained by Reuss is the lower limit of the actual value. Mavko et al. (2009) proposed to approximate the modulus M_{RVH} of the composite medium by using the average of the results in (A-1) and (A-2):

$$M_{RVH} = \frac{M_V + M_R}{2} \tag{A-3}$$

It is generally believed that the fluid medium contains water and gas, so the volume modulus K_f of the fluid phase can be similarly calculated, which is the equivalent average of the two

$$K_{\rm f} = \left(\frac{S_{\rm g}}{K_{\rm g}} + \frac{S_{\rm w}}{K_{\rm w}}\right)^{-1} \tag{A-4}$$

where, K_W and K_g are the volume modulus of water and gas respectively, S_W and S_g are the volume fraction of water and gas respectively.

When hydrate and rock particles are cemented together as part of the solid skeleton, the porosity ϕ of the rock skeleton is reduced and the elastic modulus of the solid phase is changed. When hydrate saturation is S_h , new rock porosity ϕ_r becomes

$$\phi_{\rm r} = \phi(1 - S_{\rm h}) \tag{A-5}$$

According to Hill's average (Hill, 1965), the volume modulus $K_{\rm g}$ and the shear modulus $G_{\rm g}$ of the changed solid phase can be respectively written as

$$\begin{split} K_{\rm g} &= \frac{1}{2} \left(f_{\rm h} K_{\rm h} + (1-f_{\rm h}) K_{\rm S} + \left[\frac{f_{\rm h}}{K_{\rm h}} + \frac{1-f_{\rm h}}{K_{\rm S}} \right]^{-1} \right) \\ G_{\rm g} &= \frac{1}{2} \left(f_{\rm h} G_{\rm h} + (1-f_{\rm h}) G_{\rm S} + \left[\frac{f_{\rm h}}{G_{\rm h}} + \frac{1-f_{\rm h}}{G_{\rm S}} \right]^{-1} \right) \end{split} \tag{A-6}$$

where, $f_h = \frac{\phi S_h}{1-\phi(1-S_h)}$, K_s and G_s are respectively the volume modulus and the shear modulus of pure rock solid phase, K_h and G_h are respectively the volume modulus and the shear modulus of purely natural gas hydrate.

There is a critical porosity in hydrate reservoir porosity, which is generally 36%–40%. When the actual porosity ϕ is greater than the critical porosity ϕ_c , fluid is the main carrier of wave propagation. When the actual porosity ϕ is less than the critical porosity ϕ_c , the solid is the main carrier of wave propagation (Dvorkin et al., 2003).

With the critical porosity ϕ_c , the equivalent volume modulus K_{HM} and the equivalent shear modulus G_{HM} of the rock skeleton are as follows (Mindlin, 1949):

$$\begin{split} K_{HM} &= \left[\frac{n^2 (1 - \phi_{\text{c}})^2 K_{\text{g}}^2}{18\pi^2 (1 - \nu_{\text{g}})^2} P \right]^{1/3} \\ G_{HM} &= \frac{5 - 4\nu_{\text{g}}}{5(2 - \nu_{\text{g}})} \left[\frac{3n^2 (1 - \phi_{\text{c}})^2 G_{\text{g}}^2}{2\pi^2 (1 - \nu_{\text{g}})^2} P \right]^{1/3} \end{split} \tag{A-7}$$

where, K_g and G_g are respectively the volume modulus and the shear modulus of the solid phase after the change, n is the average number of contact points of rock particles, which is generally considered to be nine, and ν_g is the changed Poisson's ratio of solid-phase:

$$v_{\rm g} = (3K_{\rm g} - 2G_{\rm g})/(6K_{\rm g} + 2G_{\rm g})$$
 (A-8)

The variable P is the effective pressure of sedimentary rock strata at a certain depth, expressed as

$$P = (1 - \phi) \left(\rho_{\rm S} - \rho_{\rm f} \right) gh \tag{A-9}$$

In (A-9), $\rho_{\rm s}$ and $\rho_{\rm f}$ are densities of the solid phase and fluid phase, respectively, g is the acceleration of gravity and h is the depth. $K_{\rm dry}$ and $G_{\rm dry}$ are respectively the equivalent volume modulus and the equivalent shear modulus of the rock skeleton without fluid (Hashin and Shtrikman, 1963)

$$K_{\text{dry}} = \left[\frac{(\phi/\phi_{\text{c}})}{K_{\text{HM}} + \frac{4}{3}G_{\text{HM}}} + \frac{(1 - \phi/\phi_{\text{c}})}{K_{\text{g}} + \frac{4}{3}G_{\text{HM}}} \right]^{-1} - \frac{4}{3}G_{\text{HM}}$$

$$G_{\text{dry}} = \left[\frac{(\phi/\phi_{\text{c}})}{G_{\text{HM}} + Z} + \frac{(1 - \phi/\phi_{\text{c}})}{G_{\text{g}} + Z} \right]^{-1} - Z$$

$$Z = \frac{G_{\text{HM}}}{6} \left(\frac{9K_{\text{HM}} + 8G_{\text{HM}}}{K_{\text{HM}} + 2G_{\text{HM}}} \right)$$
(A-10)

Then according to the Gassmann equation (Gassmann, 1951), the volume modulus and the shear modulus of hydrate reservoirs can be obtained

$$K_{\text{Sat}} = K_{\text{g}} \frac{\phi_{\text{r}} K_{\text{dry}} - (1 - \phi_{\text{r}}) K_{\text{f}} K_{\text{dry}} / K_{\text{g}} + K_{\text{f}}}{(1 - \phi_{\text{r}}) K_{\text{f}} + \phi_{\text{r}} K - K_{\text{f}} K_{\text{dry}} / K_{\text{g}}}$$
(A-11)

$$G_{\text{sat}} = G_{\text{dry}}$$

The P-wave velocity, S-wave velocity, and density in a reservoir can be calculated according to the volume modulus and the shear modulus (Ecker et al., 2000):

$$\begin{split} V_P &= \sqrt{\left(K_{\text{Sat}} + \frac{4}{3}G_{\text{Sat}}\right) / \rho} \\ V_S &= \sqrt{G_{\text{sat}}/\rho} \\ \rho &= \rho_{\text{f}}\phi_{\text{r}} + \rho_{\text{S}}(1 - \phi_{\text{r}}) \end{split} \tag{A-12}$$

Appendix B. Brekhovskikh equation

When discussing the propagation process of wave in a multilayer medium, it is usually assumed that the media on both sides of the interface are in close contact, that is, the continuity of the displacement component and stress component at the interface is satisfied. The model in Fig. B-1 shows the transmission and reflection of plane simple harmonics in thin-layer media.

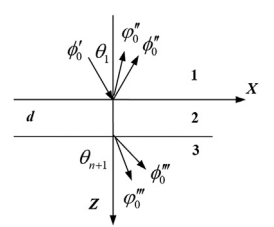


Fig. B-1. Reflection and transmission in thin layer media.

According to the continuity assumption of displacement and stress components on the interface, the relationship between displacement and stress on the bottom interface of the first layer medium and the top interface of the third layer medium is deduced as follows (Brekhovskikh, 1987):

$$\begin{bmatrix} V_X^{(3)} \\ V_Z^{(3)} \\ \sigma_{ZZ}^{(3)} \\ \frac{1}{2\mu_2} \sigma_{ZX}^{(3)} \end{bmatrix} = \begin{bmatrix} a_{11} & a_{12} & a_{13} & a_{14} \\ a_{21} & a_{22} & a_{23} & a_{24} \\ a_{31} & a_{32} & a_{33} & a_{34} \\ a_{41} & a_{42} & a_{43} & a_{44} \end{bmatrix} \begin{bmatrix} V_X^{(1)} \\ V_Z^{(1)} \\ \sigma_{ZZ}^{(1)} \\ \frac{1}{2\mu_2} \sigma_{ZX}^{(1)} \end{bmatrix}$$
(B-1)

In Eq. (B-1), the variables are expressed as follows:

$$a_{11} = 2\sin^2\gamma_2\cos P + \cos 2\gamma_2\cos Q$$

$$a_{12} = i(\tan \theta_2 \cos 2\gamma_2 \sin P - \sin 2\gamma_2 \sin Q)$$

(A-10)
$$a_{13} = \frac{\sin \theta_2}{\rho_2 V_{P2}} (\cos Q - \cos P)$$

$$a_{14} = -2iV_{S2}(\tan \theta_2 \sin \gamma_2 \sin P + \cos \gamma_2 \sin Q)$$

$$a_{21} = i \left(\frac{V_{S2} \cos \theta_2}{V_{P2} \cos \gamma_2} \sin 2\gamma_2 \sin P - \tan \gamma_2 \cos 2\gamma_2 \sin Q \right)$$

$$a_{22} = \cos 2\gamma_2 \cos P + 2 \sin^2 \gamma_2 \cos Q$$

$$a_{23} = -\frac{i}{\rho_2 V_{P2}} (\cos \theta_2 \sin P + \tan \gamma_2 \sin \theta_2 \sin Q)$$

$$a_{24} = 2V_{S2} \sin \gamma_2 (\cos Q - \cos P)$$

$$a_{31} = 2\rho_2 V_{S2} \sin \gamma_2 \cos 2\gamma_2 (\cos Q - \cos P)$$

$$a_{32} = -i\rho_2 \left(\frac{V_{P2}\cos^2 2\gamma_2}{\cos \theta_2} \sin P + 4V_{S2}\cos \gamma_2 \sin^2 \gamma_2 \sin Q \right)$$

$$a_{33} = \cos 2\gamma_2 \cos P + 2\sin^2\gamma_2 \cos Q$$

$$a_{34} = 2i\rho_2 V_{52}^2(\cos 2\gamma_2 \tan \theta_2 \sin P - \sin 2\gamma_2 \sin Q)$$

$$a_{41} = -i \left(\frac{2}{V_{P2}} \cos \theta_2 \sin^2 \gamma_2 \sin P + \frac{\cos^2 2\gamma_2}{2V_{S2} \cos \gamma_2} \sin Q \right)$$

$$a_{42} = \frac{\sin \theta_2 \cos 2\gamma_2}{V_{P2}} (\cos Q - \cos P)$$

$$a_{43} = \frac{i}{2\rho_2} \left(\frac{\sin 2\theta_2}{V_{P2}^2} \sin P - \frac{\cos 2\gamma_2}{V_{S2}^2} \tan \gamma_2 \sin Q \right)$$

$$a_{44} = 2\sin^2\gamma_2\cos P + \cos 2\gamma_2\cos Q$$

$$P = \frac{\omega d}{V_{P2}} \cos \theta_2, \ Q = \frac{\omega d}{V_{S2}} \cos \gamma_2$$

The potential function relations of the first layer and the third layer media are substituted into the above equation. $R_{PP} = \frac{\phi^{"}}{\phi^{'}}$ is Pwave reflection coefficient, $R_{PS} = \frac{\varphi''}{\phi}$ is S-wave reflection coefficient, $T_{PP} = \frac{\phi'''}{\phi'}$ is P-wave transmission coefficient, and $T_{PS} = \frac{\phi'''}{\phi'}$ is S-wave transmission coefficient. The relationship between PP and PS coefficients are be written. efficients can be written as

$$\begin{bmatrix} m_{11} & m_{12} & m_{13} & m_{14} \\ m_{21} & m_{22} & m_{23} & m_{24} \\ m_{31} & m_{32} & m_{33} & m_{34} \\ m_{41} & m_{42} & m_{43} & m_{44} \end{bmatrix} \begin{bmatrix} R_{PP} \\ R_{PS} \\ T_{PP} \\ T_{PS} \end{bmatrix} = \begin{bmatrix} n_1 \\ n_2 \\ n_3 \\ n_4 \end{bmatrix}$$
(B-2a)

In the above equation, components are expressed as

$$\begin{bmatrix} m_{11} \\ m_{21} \\ m_{31} \\ m_{41} \end{bmatrix} = \begin{bmatrix} a_{11} & a_{12} & a_{13} & a_{14} \\ a_{21} & a_{22} & a_{23} & a_{24} \\ a_{31} & a_{32} & a_{33} & a_{34} \\ a_{41} & a_{42} & a_{43} & a_{44} \end{bmatrix} \begin{bmatrix} \sin \theta_1 \\ \cos \theta_1 \end{bmatrix}$$

$$-\rho_1 V_{P1} \left(1 - 2 \frac{V_{S1}^2}{V_{P1}^2} \sin^2 \theta_1 \right)$$

$$-\frac{\rho_1 V_{S1}^2}{2\rho_2 V_{S2}^2 V_{P1}} \sin 2\theta_1$$
The relationship among other parameters of the relationshi

$$\begin{bmatrix} m_{12} \\ m_{22} \\ m_{32} \\ m_{42} \end{bmatrix} = \begin{bmatrix} a_{11} & a_{12} & a_{13} & a_{14} \\ a_{21} & a_{22} & a_{23} & a_{24} \\ a_{31} & a_{32} & a_{33} & a_{34} \\ a_{41} & a_{42} & a_{43} & a_{44} \end{bmatrix} \begin{bmatrix} -\frac{V_{P1}}{V_{S1}} \cos \gamma_1 \\ \sin \theta_1 \\ -\rho_1 V_{P1} \sin 2\gamma_1 \\ \frac{\rho_1 V_{P1}}{2\rho_2 V_{S2}^2} \cos 2\gamma_1 \end{bmatrix}$$
(B-2c)

$$\begin{bmatrix} m_{13} \\ m_{23} \\ m_{33} \\ m_{43} \end{bmatrix} = \begin{bmatrix} -\sin \theta_1 \\ \frac{V_{P1}}{V_{P3}} \cos \theta_3 \\ \rho_3 V_{P1} \left(1 - 2 \frac{V_{53}^2}{V_{P3}^2} \sin^2 \theta_3 \right) \\ -\frac{\rho_3 V_{53}^2 V_{P1}}{2\rho_2 V_{52}^2 V_{P3}^2} \sin 2\theta_3 \end{bmatrix}$$
(B-2d)

$$\begin{bmatrix} m_{14} \\ m_{24} \\ m_{34} \\ m_{44} \end{bmatrix} = \begin{bmatrix} -\frac{V_{P1}}{V_{S3}} \cos \gamma_3 \\ -\sin \theta_1 \\ -\rho_3 V_{P1} \sin 2\gamma_3 \\ -\frac{\rho_3 V_{P1}}{2\rho_2 V_{S2}^2} \cos 2\gamma_3 \end{bmatrix}$$
(B-2e)

$$\begin{bmatrix} n_1 \\ n_2 \\ n_3 \\ n_4 \end{bmatrix} = \begin{bmatrix} a_{11} & a_{12} & a_{13} & a_{14} \\ a_{21} & a_{22} & a_{23} & a_{24} \\ a_{31} & a_{32} & a_{33} & a_{34} \\ a_{41} & a_{42} & a_{43} & a_{44} \end{bmatrix} \begin{bmatrix} -\sin \theta_1 \\ \cos \theta_1 \\ \rho_1 V_{P1} \left(1 - 2 \frac{V_{S1}^2}{V_{P1}^2} \sin^2 \theta_1 \right) \\ -\frac{\rho_1 V_{S1}^2}{2\rho_2 V_{S2}^2 V_{P1}} \sin 2\theta_1 \end{bmatrix}$$

$$(B-2f)$$

$$\Delta_{1} = \begin{vmatrix} n_{1} & m_{12} & m_{13} & m_{14} \\ n_{2} & m_{22} & m_{23} & m_{24} \\ n_{3} & m_{32} & m_{33} & m_{34} \\ n_{4} & m_{42} & m_{43} & m_{44} \end{vmatrix}, \Delta_{2} = \begin{vmatrix} m_{11} & n_{1} & m_{13} & m_{14} \\ m_{21} & n_{2} & m_{23} & m_{24} \\ m_{31} & n_{3} & m_{33} & m_{34} \\ m_{41} & n_{4} & m_{43} & m_{44} \end{vmatrix}$$
(B-2g)

$$\Delta_{3} = \begin{vmatrix} m_{11} & m_{12} & n_{1} & m_{14} \\ m_{21} & m_{22} & n_{2} & m_{24} \\ m_{31} & m_{32} & n_{3} & m_{34} \\ m_{41} & m_{42} & n_{4} & m_{44} \end{vmatrix}, \Delta_{4} = \begin{vmatrix} m_{11} & m_{12} & m_{13} & n_{1} \\ m_{21} & m_{22} & m_{23} & n_{2} \\ m_{31} & m_{32} & m_{33} & n_{3} \\ m_{41} & m_{42} & m_{43} & n_{4} \end{vmatrix}$$
 (B-2h)

$$R_{PP} = \frac{\Delta_1}{|M|} \quad R_{PS} = \frac{\Delta_2}{|M|} \quad T_{PP} = \frac{\Delta_3}{|M|} \quad T_{PS} = \frac{\Delta_4}{|M|}$$
 (B-3)

The relationship among other parameters can be expressed as

$$P = \alpha_2 d, Q = \beta_2 d \tag{B-4a}$$

$$k_{1} = \frac{\omega}{V_{P1}}, k_{1}^{'} = \frac{\omega}{V_{S1}}, k_{2} = \frac{\omega}{V_{P2}}, k_{2}^{'} = \frac{\omega}{V_{S2}}, k_{3} = \frac{\omega}{V_{P3}}, k_{3}^{'} = \frac{\omega}{V_{S3}}$$
(B-4b)

and $\sigma = k_1 \sin \theta_1 = k_n \sin \theta_n = k_1' \sin \gamma_1 = k_n' \sin \gamma_n$, Snell's law holds.

Other variables are expressed as

$$\alpha_1 = (k_1^2 - \sigma^2)^{1/2} = k_1 \cos \theta_1, \beta_1 = (k_1'^2 - \sigma^2)^{1/2} = k_1' \cos \gamma_1$$
(B-5a)

$$\alpha_2 = (k_2^2 - \sigma^2)^{1/2} = k_2 \cos \theta_2, \ \beta_2 = (k_2^2 - \sigma^2)^{1/2} = k_2^{\prime} \cos \gamma_2$$
(B-5b)

$$\alpha_3 = \left(k_3^2 - \sigma^2\right)^{1/2} = k_3 \cos \theta_3, \ \beta_3 = \left(k_3^{'2} - \sigma^2\right)^{1/2} = k_3^{'} \cos \gamma_3$$
(B-5c)

$$\begin{split} &\lambda_1 {K_1}^2 + 2\mu_1 {\alpha_1}^2 = \rho_1 \omega^2 \cos 2\gamma_1 \\ &2\mu_1 \sigma \beta_1 = \rho_1 \omega^2 \sin 2\gamma_1 \\ &\left(\sigma^2 - {\beta_1}^2\right) = -\left(\omega^2 \cos 2\gamma_1\right) \Big/ V_{S1}^2 \end{split} \tag{B-5d}$$

where, V_{P1} , V_{P2} , and V_{P3} are the P-wave velocities of the three layers, respectively; V_{S1} , V_{S2} , and V_{S3} are the S-wave velocities of the three layers; ρ_1 , ρ_2 , and ρ_3 are the density of three layers; d is the thickness of the second layer of the medium; ω is the angular frequency; θ_1 , θ_2 , θ_3 and γ_1 , γ_2 , γ_3 are respectively the incidence angles of the P-wave and the S-wave in three layers; ϕ' , ϕ'' , ϕ''' and ϕ' , ϕ'' , ϕ''' are respectively the potential functions of the P-wave and the S-wave in three layers; α is the vertical component of the longitudinal wave number k in the layer, β is the vertical component of the transverse wave number k in the layer, α is the phase velocity of the wave along with the interface; λ , K and μ are the moduli of elasticity.

References

Andreassen, K., Hart, P.E., Mackay, M., 1997. Amplitude versus offset modelling of the bottom simulating reflection associated with submarine gas hydrates[J]. Mar. Geol. 137 (1–2), 25–40. https://doi.org/10.1016/S0025-3227(96)00076-X.

Arun, K.P., Sain, K., Kumar, J., 2020. Application of constrained AVO inversion: 2-D modelling of gas hydrates and free gas in Mahanadi basin, India. J. Nat. Gas Sci. Eng. 78, 103287. https://doi.org/10.1016/j.jngse.2020.103287.

Breiman, L., 2001. Random forest. Mach. Learn. 45, 5–32. https://doi.org/10.1023/A: 1010933404324.

Brekhovskikh, L., 1987. Mechanics of continua and wave dynamics. J. Acoust. Soc. Am. 82 (1), 400. https://doi.org/10.1121/1.395509.

Chen, S., Lu, R., Liu, L.H., et al., 2020. Analysis of the influence of thin interbed interference on pre-stack AVO attributes. Earth Sci. Front. 27 (4). https://doi.org/ 10.13745/j.esf.sf.2020.4.26, 098-109. Dvorkin, J., Nur, A., Uden, R., et al., 2003. Rock physics of a gas hydrate reservoir. Lead. Edge 22 (9), 842–847. https://doi.org/10.1190/1.1614153.

Ecker, C., Dvorkin, J., Nur, A., 1998. Sediments with gas hydrates: internal structure from seismic AVO. Geophysics 63 (5), 1659–1669. https://doi.org/10.1190/

Ecker, C., Dvorkin, J., Nur, A., 2000. Estimating the amount of gas hydrate and free gas from marine seismic data. Geophysics 65 (2), 565–573. https://doi.org/10.1190/1.1444752.

Gassmann, F., 1951. Elastic waves through a packing of spheres. Geophysics 16 (4), 673–685. https://doi.org/10.1190/1.1437718.

Hashin, Z., Shtrikman, S., 1963. A variational approach to the theory of the elastic behaviour of multiphase materials. J. Mech. Phys. Solid. 11 (2), 127–140. https:// doi.org/10.1016/0022-5096(63)90060-7.

Hill, R., 1965. A self-consistent mechanics of composite materials. J. Mech. Phys. Solid. 13 (4), 213–222. https://doi.org/10.1016/0022-5096(65)90010-4.

Lu, S.Q., 2013. Application of pre-stack frequency division AVO analysis method in Luojia area. Geophys. Prospect. Pet. 52, 2. https://doi.org/10.3969/j.issn.1000-1441.2013.02.006.

Lu, S., Mcmechan, G.A., 2004. Elastic impedance inversion of multichannel seismic data from unconsolidated sediments containing gas hydrate and free gas. Geophysics 69 (1), 164–179. https://doi.org/10.1190/1.1649385.

Mallick, S., Huang, X., Lauve, J., et al., 2000. Hybrid seismic inversion: a reconnaissance tool for deep-water exploration. Lead. Edge 19 (11), 1230–1237. https://doi.org/10.1190/1.1438512.

Mavko, G., Mukerji, T., Dvorkin, J., 2009. The Rock Physics Handbook. Cambridge University Press, Cambridge, UK, ISBN 9780521861366.

Meng, X.J., et al., 2010. The phase angle change for seismic reflection coefficient. OG 45 (Suppl. 1), 121–124. CNKI:SUN:SYDO.0.2010-S1-026.

Mindlin, R.D., 1949. Compliance of elastic bodies in contact. J. Appl. Mech. 16, 259–268. https://doi.org/10.1007/978-1-4613-8865-4_24.

Reuss, A.Z., 2006. Berechnung der Fliessgrenze von Mischkristallen auf Grund der Plastizitätsbedingung für Einkristalle. Z Angew Math Mech 9:49-58[J]. Zamm Journal of Applied Mathematics & Mechanics Ztschrift Fur Angewandte Mathematik Und Mechanik 9 (1), 49–58. https://doi.org/10.1002/zamm.19290090104.

Robinson, E.A., 1967. Predictive decomposition of time series with application to seismic exploration. Geophysics 32 (3), 418–484. https://doi.org/10.1190/11439873

Salehi, E., Javaherian, A., Pour, M.A., et al., 2013. Quantitative seismic pre-stack analysis of potential gas-hydrate resources in the Makran Accretionary Prism, offshore Iran. Mar. Petrol. Geol. 48, 160–170. https://doi.org/10.1016/ i.marpetgeo.2013.07.015.

Shuey, R.T., 1985. A simplification of the Zoeppritz equations. Geophysics 50 (4), 609–614. https://doi.org/10.1190/1.1441936.

Tessmer, E., Kosloff, D., Behle, A., 1992. Elastic wave propagation simulation in the presence of surface topography. Geophysics 108, 621–632, 0.1111/j.1365-246X.1992.tb04641.x.

Voigt, W., 1889. Über die Beziehung zwischen den beiden Elatiziä tskonstanten isotroper Körper. Wied Ann 38, 572. https://doi.org/10.1002/andp.18892741206.
 Wang, J.H., 2006. A New Method on Prestack Elastic Parameters Inversion. In: Doctoral Dissertation. Ocean University of China, Qingdao.

Wang, Y.F., Cui, Y., Yang, C.C., 2011. Hybrid regularization methods for seismic reflectivity inversion. International Journal on Geomathematics 2, 87–112. https://doi.org/10.1007/s13137-011-0014-1.

Yi, B.Y., Lee, C.H., 2011. Qualitative assessment of gas hydrate and gas concentrations from the AVO characteristics of the BSR in the Ulleung Basin, East Sea (Japan Sea). Mar. Petrol. Geol. 28, 1953–1966. https://doi.org/10.1016/j.marpetgeo.2010.12.001.

Yi, B.Y., Lee, G.H., Kang, Nyeon, K., Yoo, Dong, G., Lee, Joo, Y., 2018. Deterministic estimation of gas-hydrate resource volume in a small area of the Ulleung Basin, East Sea (Japan Sea) from rock physics modelling and prestack inversion. Mar. Petrol. Geol. 92, 597—608, 10.1016/j.marpetgeo.2017.11.023.

Zoeppritz, K., 1919. Erdbebenwellen VII. Über Reflexion und Durchgang seismischer Wellen durch Unstetigkeitsfl achen. Nachrichten der Koniglichen Gesellschaft der Wissenschaften zu Gottingen.